

Analysis of the 3C 445 soft X-ray spectrum as observed by *Chandra* high-energy gratings

Fu-Tong Dong¹, Shu-Hua Shao¹, Yan Cheng¹ and Jiao-Long Zeng²

¹ Technological Vocational College of Dezhou, Dezhou 251200, China; dongfutong@sohu.com

² College of Science, National University of Defense Technology, Changsha 410073, China

Received 2017 December 12; accepted 2018 February 4

Abstract We present a detailed analysis of the soft X-ray emission of 3C 445 using an archival *Chandra* High Energy Transmission Grating (HETG) spectrum. Highly-ionized H- and He-like Mg, Si and S lines, as well as a resolved low-ionized Si $K\alpha$ line, are detected in the high resolution spectrum. The He-like triplets of Mg and Si are resolved into individual lines, and the calculated R ratios indicate a high density for the emitter. The low values of G ratios indicate the lines originate from collisionally ionized plasmas. However, the detection of a resolved narrow Ne X radiative recombination continua (RRC) feature in the spectrum seems to prefer a photoionized environment. The spectrum is subsequently modeled with a photoionization model, and the results are compared with those of a collisional model. Through a detailed analysis of the spectrum, we exclude a collisional origin for these emission lines. A one-component photoionization model provides a great fit to the emission features. The best-fit parameters are $\log \xi = 3.3_{-0.3}^{+0.4} \text{ erg cm s}^{-1}$, $n_{\text{H}} = 5_{-4.5}^{+15} \times 10^{10} \text{ cm}^{-3}$ and $N_{\text{H}} = 2.5_{-1.7}^{+3.8} \times 10^{20} \text{ cm}^{-2}$. According to the calculated high density for the emitter, the measured velocity widths of the emission lines and the inferred radial distance ($6 \times 10^{14} - 8 \times 10^{15} \text{ cm}$), we suggest the emission lines originating from matter are located in the broad line region (BLR).

Key words: galaxies: active — X-rays: galaxies — galaxies: individual (3C 445)

1 INTRODUCTION

With the development of high resolution observations of active galactic nuclei (AGNs), more and more emission features have been observed in the associated soft X-ray spectra. Emission features revealed by a high resolution spectrum, e.g. the radiative recombination continua (RRC) and the He-like triplets, are normally identified as emission from highly ionized H- and He-like ions of astrophysically abundant elements (e.g. NGC 3783, Kaspi et al. 2001; NGC 1068, Kinkhabwala et al. 2002; NGC 4151, Armentrout et al. 2007). Modeling these features with theoretical models has proved to be a powerful tool for diagnosing the physical process of generating these emission features (i.e. collisional ionization or photoionization), and inferring the physical properties of the line emitting gas, e.g. electron density, column density and their distribution around the central region (Young et al. 2001; Bianchi et al. 2006; Kraemer et al. 2008).

3C 445 ($z = 0.0562$) is classified as a broad line radio galaxy (BLRG) with an FR II morphology (Kronberg et al. 1986). The central engines of radio-loud objects have been poorly studied so far due to the relative rarity and far distance of these sources. The soft X-ray emission lines, however, provide a useful way of interpreting their inner environment. To date, several BLRG objects have been observed with soft X-ray emission lines, for instance: 3C 33 (Torresi et al. 2009), 3C 234 (Piconcelli et al. 2008) and 3C 445 (Sambruna et al. 2007; Reeves et al. 2010; Braitto et al. 2011).

3C 445 is an ideal target for investigating the nature of the central engines of radio-loud objects. High resolution observations have revealed a multitude of soft X-ray emission features from H- and He-like ions in this object. The *XMM-Newton* RGS spectra provided the first detection of the O VII and O VIII emission lines (Grandi et al. 2007). These lines are considered most likely to

be from a warm photoionized gas. However, the relatively low resolution and short exposure time restrict an accurate measurement of the line parameters. The subsequent *Chandra* Low Energy Transmission Grating (LETG) spectrum of 3C 445 detected and resolved emission lines from H- and He-like O, Ne, Mg and Si ions (Reeves et al. 2010). This spectrum gives the first detailed measurement of soft X-ray emission from this object. Based on the emission features from O VII and O VIII, Reeves et al. (2010) inferred that the emission comes from photoionized gas which probably is located in the broad line region (BLR).

The most recent *Chandra* High Energy Transmission Grating (HETG) spectrum provides some distinct emission features in the soft X-ray band compared to previous observations, e.g. resolved Mg XI and Si XIII triplets. These new characteristics may provide more accurate constraints on the physical states of the line emitting gas. As far as we know, no research on the soft X-ray emission has been published in the literature based on these data. Consequently, in this paper, we investigate the soft X-ray emission of 3C 445 in detail based on the spectrum observed by *Chandra* HETG. Our goal is to analyze the soft X-ray emission features in the spectrum and to make a detailed comparison with those obtained with the *Chandra* LETG spectrum (Reeves et al. 2010), in order to better understand the physical properties of the soft X-ray emitting gas.

2 DATA REDUCTION

The HETG onboard *Chandra* observed 3C 445 from 2011 July 25 to 2011 August 9. These data were obtained from the *Chandra* Public Data Archive¹, with four sequences of observations: 13305, 13306, 13307 and 14194. The data were reduced with the standard CIAO 4.9 tools (Fruscione et al. 2006). In order to apply the most updated calibrations, we ran the *Chandra* reprocessing script to create new spectral files. Only the first order dispersed spectra were considered for both the medium energy grating (MEG) and high energy grating (HEG), and the ± 1 orders for each grating were subsequently combined for each sequence. As no significant variability was found between the four sequences, we combined the spectra from all the four sequences to yield a single 1st order spectrum for both the MEG and HEG, with a total exposure time of 413 ks. The spectra were used in the energy range of 1.2–5 keV for MEG and 3–8 keV for HEG. Below 1.2 keV, the signal to noise ratio

of the MEG data is very low and no significant emission line feature was detected. While above 8 keV, the HEG spectrum was not actually detected above the background. The mean count rates were 0.0117 counts s^{-1} and 0.0127 counts s^{-1} for MEG (1.2–5 keV) and HEG (3–8 keV) respectively.

The resultant time-averaged spectra were subsequently analyzed using the spectral fitting tool *Sherpa* (Freeman et al. 2001). The spectra were binned at two different levels, i.e. $\Delta\lambda = 0.005 \text{ \AA}$ and 0.01 \AA for HEG and MEG respectively, or at the full width at half maximum (FWHM) of their resolution. The former finer binning was used for the spectral fitting and line identification, while the latter was used only for the purpose of plotting. We used the *C*-statistic (Cash 1979) for the subsequent spectral fit, as the counts per bin drop below $N < 10$ in some bins in the soft X-ray band. The error bars quoted throughout the paper correspond to the 90% confidence interval (i.e. $\Delta C = 2.706$ for one interesting parameter).

In this paper, we also used the *Chandra* LETG data for the purpose of comparison. The observation was performed from 2009 September 25 to October 3, with *Chandra* ACIS-S for a total exposure time of 200 ks. These data have been analyzed by Reeves et al. (2010). We reduced the data following the standard procedure as described above, and obtained a time-averaged spectrum with mean count rate of ~ 0.0132 counts s^{-1} in the 0.5–9 keV band.

3 LINE IDENTIFICATION

Initially, we concentrated on analysis of the MEG spectrum to search for the soft X-ray emission lines and measure their properties. As an overall preview of the emission line features, Figure 1 shows flux of the MEG spectrum fitted with a broken power-law. Since there are no significant emission lines being resolved above 2.4 keV, the spectrum was only plotted in the energy range of $\sim 1.2 - 2.4$ keV. The spectrum shown in Figure 1 clearly exhibits several strong emission line structures in the AGN rest frame, as confirmed by previous studies with the high resolution *Chandra* LETG and *XMM-Newton* spectrum (Reeves et al. 2010; Braito et al. 2011). The expected emission features in the observed frame are marked in the figure. Most of these lines are expected from H- and He-like Mg, Si and S ions. There is also a strong emission feature at ~ 1.65 keV which may be identified as the Si $K\alpha$ line.

¹ <http://cxc.harvard.edu/cda/>

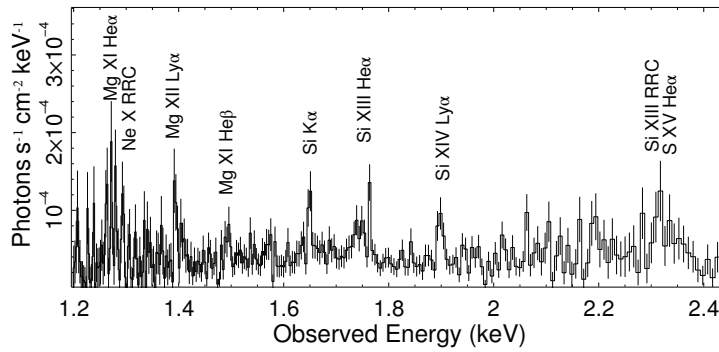


Fig. 1 Flux of the *Chandra* MEG spectrum of 3C 445 in the emission line energy band.

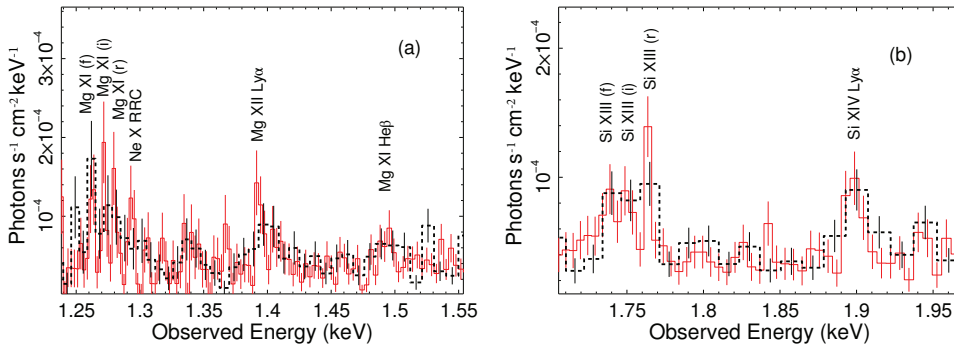


Fig. 2 *Chandra* MEG (red solid line in the electronic version) and LETG (black dashed line in the electronic version) spectra folded against a broken power-law continuum. Panel (a) shows the spectra in the Mg band. Panel (b) shows the spectra in the Si band.

Due to the low quality of data below 1.2 keV, no emission feature can be detected in the present spectrum from low-Z ions, e.g. the O VII, O VIII, Ne IX lines as observed in the LETG spectrum (Reeves et al. 2010). However, the high resolution and long exposure time guarantee the MEG spectrum resolves some emission features that have never been detected in the LETG observation.

Figure 2 shows a direct comparison of the LETG spectrum with the MEG in the Mg and Si line band. Apparently, the MEG spectrum has a better resolution for the emission lines, specifically for the He-like triplets of Mg and Si which appear to be resolved into their individual lines in the MEG spectrum, but these lines are barely resolved in the LETG spectrum. In addition, the MEG spectrum also resolves a narrow feature around 1.29 keV in the observed frame, which may be identified as the RRC from Ne X. On the contrary, no such feature is detected in the LETG spectrum.

In order to extract parameters for these emission features as accurately as possible, we fitted the spectrum using a ‘local fits’ method as described in Guainazzi & Bianchi (2007) and Nucita et al. (2010). In principle, this

method provides more accurate measurement of the line parameters than the ‘global fits’ method if the continuum is very complex, by removing any uncertainties regarding how the continuum is modeled. Previous X-ray studies of 3C 445 revealed the continuum is heavily absorbed by complex absorbing components (Sambruna et al. 2007; Braitto et al. 2011). Besides, a strong cold reflection component is also required to predict the hard excess above 10 keV and the strong Fe K α line at ~ 6.4 keV. Thus the complexity of the continuum may affect the measurement of line parameters using the ‘global fits’ method.

Upon modeling each emission feature, the spectrum is divided into intervals of width 0.1 keV which cover the selected emission feature well. The continuum can be well modeled with a simple power-law in such a narrow energy region. The lines were fitted using a Gaussian profile with the centroid energy, line width and line flux left free to vary, while the RRC profile was modeled with a recombination emission edge. Note upon modeling the He-like triplets of Mg XI and Si XIII, we assumed that the widths of the three lines of each ion were identical and tied these values in the resulting model. As for the He-like triplet of S XV, no individual line appears to

be resolved in the spectrum. Thus this component was fitted with a single Gaussian profile. The Galactic absorption was accounted for in the spectral analysis by using the neutral absorption model *wabs* with column density $N_{\text{H}} = 4.6 \times 10^{20} \text{ cm}^{-2}$ for 3C 445 (Dickey & Lockman 1990). The measured line fluxes, widths, equivalent widths, centroid energies and their statistical significances are listed in Table 1.

Most of the signatures are detected at a confidence level $> 99\%$, i.e. $\Delta C > 11.3$ for three parameters or $\Delta C > 9.21$ for two parameters. Specifically, the Si XIII He-like resonance, the Si XIV Ly α and the Si K α lines are detected with $\Delta C > 21.1$, which corresponds to the confidence level $> 99.99\%$. The strong Si K α line is evidently from different regions in the central engine from the highly ionized lines, due to its low ionization state. Indeed, this line most probably originates from reflection off a Compton-thick mirror (see Sect. 5).

Comparing the measured centroid energies with the expected line energies, we found that most of the line centroids are consistent with the expected values in the quoted error range, especially for the strongest and most isolated lines, such as Mg XII Ly α and Si XIV Ly α . This indicates the line emitter is most likely stationary relative to the local AGN. Indeed, evidence of zero velocity shift for the soft X-ray emitter has also been suggested by the *Chandra* LETG spectrum (Reeves et al. 2010).

As discussed in Braitto et al. (2011), because the flux state is rather constant for 3C 445, we could compare the present line fluxes with those measured with the *Chandra* LETG spectrum (Reeves et al. 2010).

Figure 3 shows the flux differences of Mg and Si lines between the MEG and LETG spectra. Good agreements are achieved for the H-like Mg XII Ly α and Si XIV Ly α lines, i.e. $\sim 10\%$ difference for Mg XII Ly α between the two observations, and $< 10\%$ for Si XIV Ly α . The He α (i)+(r) fluxes are consistent within $< 30\%$ differences between the two observations. However, the differences are relatively large for the forbidden lines in the He-like triplets, e.g. the flux of the Mg XI He α (f) line in LETG is more than twice that of MEG. The difference is probably because individual lines in the He-like triplets of Mg XI and Si XIII are poorly resolved in the LETG spectrum as shown in Figure 2.

The line widths of the two prominent H-like Mg XII Ly α and Si XIV Ly α lines were well determined. The Mg XII Ly α line was resolved with a width of $\sigma = 2.0_{-0.8}^{+1.7} \text{ eV}$ and the Si XIV Ly α with $\sigma = 2.5_{-2}^{+3.3} \text{ eV}$, corresponding to FWHM widths of $1000_{-400}^{+800} \text{ km s}^{-1}$ and

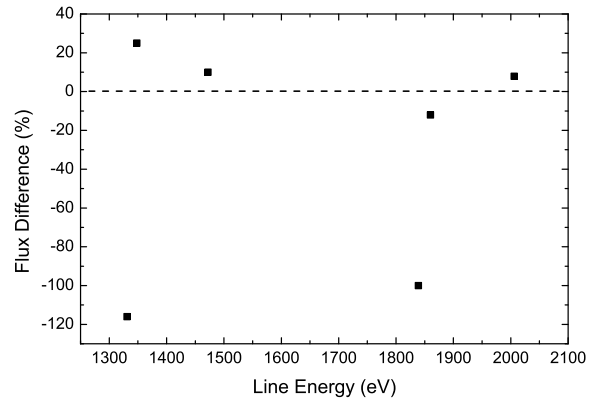


Fig. 3 Flux difference of Mg and Si lines between the MEG and LETG spectra. Note the He α (i) and (r) lines of Mg XI and Si XIII were not resolved in the LETG spectrum, thus we compared the total flux (i.e. (i) + (r)) in each triplet between the two observations.

$900_{-700}^{+1200} \text{ km s}^{-1}$ respectively. However, only upper limits were obtained for the intrinsic velocity widths for the He-like Mg XI and Si XIII lines, i.e. $\sigma < 2 \text{ eV}$ and $\sigma < 3 \text{ eV}$ (corresponding to FWHM widths of $< 1100 \text{ km s}^{-1}$ and $< 1200 \text{ km s}^{-1}$) respectively. Comparing the soft X-ray line FWHM with that of the H β line can potentially give a direct indication of the location of the soft X-ray line-emitting region relative to the optical BLR. We used the method described in Shu et al. (2010, 2011).

Figure 4 shows the FWHM ratios of the Mg XII Ly α and Si XIV Ly α lines with that of the H β line (FWHM $\sim 3000 \text{ km s}^{-1}$, Osterbrock et al. 1976; Eracleous & Halpern 2004). We found, at the two-parameter 99% confidence level, both of the FWHM ratios were consistent with 1. This indicates the soft X-ray line gas may have the same location as the BLR gas.

3.1 Radiative Recombination Continua

The MEG spectrum detected a distinct Ne X RRC feature that can be used as a temperature diagnostic for the plasmas. Although a feature is apparent near the expected energy of Si XIII RRC (see Fig. 1), it is too heavily blended with the surrounding emission (S XV He α) for us to be able to resolve the width, and hence it is not used here. The RRC feature is formed by a free electron recombined directly into an ion. The energy of the free electron is sensitive to the electron temperature of the emitting gas, therefore the RRC feature will have different structures for plasmas with different temperatures. RRC features originating in hot plasmas are broad and blurred, while the features are narrow and prominent for

Table 1 Summary of Line Parameters detected on the MEG Spectrum

Line ID	Line Energy (eV) ^a	Flux (10^{-7} photons $\text{cm}^{-2} \text{s}^{-1}$) ^b	σ or kT_e (eV) ^c	EW (eV) ^d	ΔC ^e	E_{exp} (eV) ^f
Mg XI He α (r)	1352 ⁺¹ ₋₁	4.8 ^{+3.3} _{-2.5}	< 2	13.9 ^{+9.5} _{-7.2}	12	1352
Mg XI He α (i)	1343 ⁺¹ ₋₁	5.8 ^{+3.5} _{-2.6}	---	11.6 ^{+6.9} _{-5.3}	19	1344
Mg XI He α (f)	1334 ⁺¹ ₋₁	5.1 ^{+3.6} _{-2.8}	---	11.5 ^{+8.2} _{-6.4}	11	1331
Ne X RRC	1365 ⁺¹ ₋₂	4.1 ^{+3.1} _{-2.3}	< 4	9.3 ^{+7.1} _{-5.2}	11	1362
Mg XII Ly α	1472 ⁺² ₋₁	6.7 ^{+3.8} _{-3.1}	2.0 ^{+1.7} _{-0.8}	17.3 ^{+9.2} _{-7.5}	18	1472
Mg XI He β	1578 ⁺³ ₋₃	4.2 ^{+3.0} _{-2.5}	3.6 ^{+3.4} _{-3.6}	10.5 ^{+7.6} _{-5.3}	10	1579
Si K α	1742 ⁺² ₋₁	7.2 ^{+3.3} _{-2.7}	1.9 ^{+1.8} _{-1.3}	15.8 ^{+7.3} _{-6.0}	25	1744 ^g
Si XIII He α (r)	1863 ⁺¹ ₋₁	6.7 ^{+2.8} _{-2.3}	< 3	15.8 ^{+6.7} _{-5.4}	35	1865
Si XIII He α (i)	1847 ⁺⁴ ₋₂	3.1 ^{+2.5} _{-1.8}	---	7.2 ^{+6.0} _{-4.3}	10	1854
Si XIII He α (f)	1837 ⁺² ₋₃	4.0 ^{+2.9} _{-2.1}	---	9.4 ^{+6.8} _{-4.8}	14	1839
Si XIV Ly α	2005 ⁺³ ₋₂	7.6 ^{+4.3} _{-3.0}	2.5 ^{+3.3} _{-2.0}	19.6 ⁺¹¹ _{-7.7}	24	2006
S XV He α	2451 ⁺¹² ₋₁₄	19.4 ^{+14.6} _{-13.3}	14.0 ^{+15.6} _{-13.9}	36.9 ^{+27.8} _{-25.3}	11	2447

Notes: ^a The measured line centroid energy; ^b The measured line fluxes; ^c The widths of the detected lines or temperature of RRC feature; ^d Equivalent widths of the lines; ^e Improvement in C -statistic after adding the feature to the model; ^f The expected line energies taken from the CHIANTI database (Dere et al. 2001); ^g The value is calculated using the flexible atomic code (FAC) (Gu 2003).

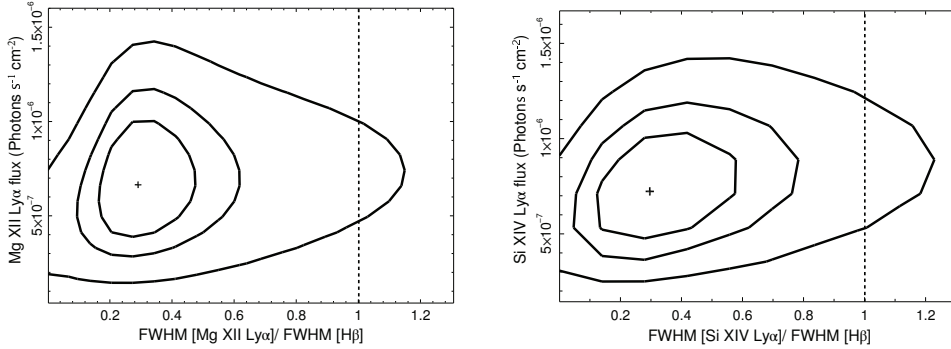


Fig. 4 Joint 68%, 90% and 99% confidence contours of the line flux versus the ratio of the line FWHM to the $H\beta$ FWHM for Mg XII Ly α and Si XIV Ly α . The vertical dashed line corresponds to the FWHM ratio equalling 1.

warm photoionized plasmas. Thus electron temperature determined from the RRC width can indicate either a photoionization or collisional-ionization environment for the line emitting gas (Liedahl & Paerels 1996; Liedahl 1999).

Using the Ne X RRC, we tried to measure the electron temperature of the line emitting gas. However the feature was found to be relatively weak with $\Delta C = 11$ for three parameters (Table 1), which means this feature is only detected at $> 98\%$ confidence. Nonetheless, an upper limit was obtained for the RRC width of < 4 eV, implying a temperature of $kT_e < 4 \times 10^4$ K for the emitting gas. This limit is consistent with the temperature derived from the *Chandra* LETG spectra using O VII and O VIII RRCs ($kT_e \sim 3 \times 10^4$ K; Reeves et al. 2010). The low temperature provides evidence of photoionization for the plasmas, as it would be insufficient for the

high-Z elements (Mg, Si and S) to be ionized to H- and He-like ions in collisionally ionized plasmas.

3.2 He-like Triplets

For the two significant He-like triplets of Mg XI and Si XIII, we present measurements of the standard plasma diagnostic ratios $R = f/i$ and $G = (i+f)/r$ (Gabriel & Jordan 1969, Gabriel & Jordan 1973; Porquet & Dubau 2000), where f , i and r are the forbidden, intercombination and resonance line fluxes respectively. The line ratios provide a diagnostic of the electron density and temperature in hot plasmas (Gabriel & Jordan 1969; Porquet et al. 2001). In the photoionized condition, Porquet & Dubau (2000) found that the R ratio is sensitive to electron density of the plasma, and the G ratio is sensitive to electron

temperature of the plasma and is a good indicator of the ionization mechanism of the line emitting gas.

The values are $R = 0.9_{-0.5}^{+1.1}$ and $1.3_{-0.7}^{+2.3}$, and $G = 2.3_{-1.1}^{+2.7}$ and $1.1_{-0.5}^{+0.8}$ for Mg XI and Si XIII respectively. Comparing these values with figure 8 in Porquet & Dubau (2000), the R ratio for Mg XI implies an electron density in the range of $n_e = 10^{12} - 10^{14} \text{ cm}^{-3}$, and an upper limit of $n_e < 10^{14} \text{ cm}^{-3}$ was obtained using Si XIII. All of these values imply a high electron density for the line emitting gas. This is consistent with measurements from the O VII triplet in the *Chandra* LETG spectrum, with the electron density $n_e > 10^{10} \text{ cm}^{-3}$ (Reeves et al. 2010). However, extracting detailed values of density is complicated by the fact that a strong ultraviolet (UV) radiation field can mimic the effect that a relatively high density has on the intercombination and forbidden line strengths (Porter & Ferland 2007).

The low values of the G ratio from both Mg XI and Si XIII indicate a collisionally ionized plasma. However, this is in contrast to the narrow Ne X RRC feature which prefers a photoionized environment. In fact, the G ratio is no longer suitable for plasma diagnostic in this case. As discussed in Kinkhabwala et al. (2002), in photoionized plasmas, a significant contribution of photoexcitation would raise the intensity of the resonance transition drastically, and causes the G ratio to act more like that in the collisionally ionized case. Moreover, optical depth in the resonance line will severely affect values of the G ratio, yielding the G ratio a function of the column density (Porter & Ferland 2007). Thus we cannot tell the difference between collisional-ionization and photoionization only with the G ratios. To further investigate this problem, we modeled the emission lines with a collisionally ionized model and compared the result with that using a photoionized model in the next section.

4 MODELING THE LINES

In modeling the emission lines, we employed a more physical model to fit the overall spectra, using both the MEG and HEG data. The continuum was modeled with a partial covering model that has been used with previous LETG and *Suzaku* data (Reeves et al. 2010; Braito et al. 2011), in the form $wabs \times ((pow1 + reflion) \times zwabs \times zpcfabs + pow2)$. Here *pow1* is an absorbed power-law representing the main radiation component from the central source, *pow2* represents part of the main radiation scattered into our line of sight by the ambient material and *reflion* is a reflection component representing the Compton mirror detected in this object. *zwabs* and *zpc-*

fabs are the intrinsic absorption components with one fully covering the central radiation and the other one partially covering it. All of the components are modified by the local Galactic absorber *wabs* with the column density of $N_H = 4.6 \times 10^{20} \text{ cm}^{-2}$. A cross normalization was adopted between the HEG and MEG spectra, and the value was always found to be consistent with 1 ($1.1_{-0.1}^{+0.1}$ for the MEG spectrum).

4.1 Collisionally Ionized Model

Initially, in order to test the ionization mechanism of the plasma, we fitted the emission lines with a collisional model using the *MEKAL* code (Mewe et al. 1986, Liedahl et al. 1995). In this model, the abundances were fixed to solar values and the redshift was fixed to the value of 3C 445 ($z = 0.0562$). The free parameters were the plasma temperature, the hydrogen density and the normalization. This model was incorporated into the continuum model given above to fit the overall (HEG + MEG) spectra, and produced an acceptable fit with the overall fit statistic $C/dof = 1467/1291$. Note the Si $K\alpha$ line was modeled separately with a single Gaussian. The fitted temperature is $kT = 0.7_{-0.1}^{+0.1} \text{ keV}$, with a high hydrogen density $n_H = 3.6_{-3.0}^{+11.5} \times 10^{13} \text{ cm}^{-3}$.

Figure 5 shows the results of the emission lines fitted by this model in the Mg and Si band. Obviously, the He-like lines of Si XIII are fitted well with this model. However, the model overpredicts the emission lines in the Mg band, especially for Mg XII $Ly\alpha$. In addition, it fails to account for the Ne X RRC (Fig. 5(a)) and the Si XIV $Ly\alpha$ line (Fig. 5(b)). For comparison, Figure 6 shows that a photoionization model fits the emission lines better than the collisional model for both the He-like and H-like lines, especially for the RRC feature. Therefore, a collisional origin appears to be excluded for the soft X-ray emission lines. This is consistent with the diagnostics of the LETG spectrum using the O VII and O VIII lines (Reeves et al. 2010).

4.2 Photoionization Model

In order to extract the physical conditions in the line emitting gas, we attempted to model the emission lines using the photoionization code CLOUDY C13.05 (Ferland et al. 2013) in this section. A plane-parallel geometry is assumed, with the slab depth controlled by the hydrogen column density parameter (N_H). The free parameters in the model are: ionization parameter (ξ), den-

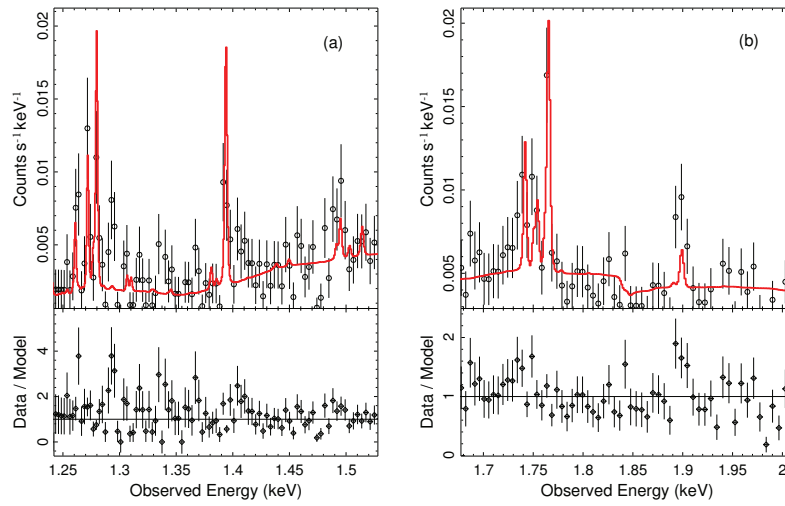


Fig. 5 The emission lines fitted with a collisional model. Panel (a) shows the spectrum in the Mg band. Panel (b) shows the spectrum in the Si band.

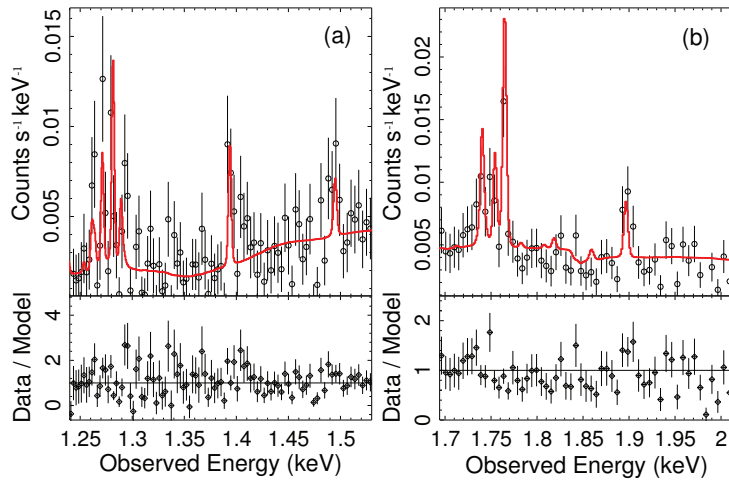


Fig. 6 The emission lines fitted with a photoionization model. Panel (a) shows the spectrum in the Mg band. Panel (b) shows the spectrum in the Si band.

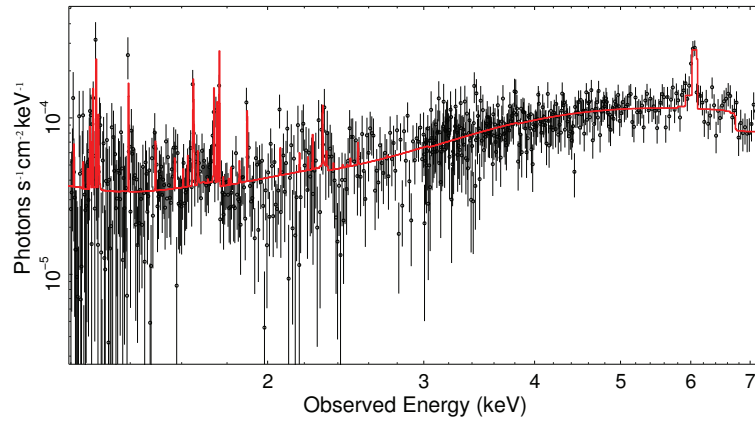


Fig. 7 The overall MEG + HEG spectrum fitted by the model described in Sect. 4.

sity of the material (n_{H}) and column density (N_{H}) of the gas.

As mentioned in the above section, the He-like emission line intensities critically depend on the spectral energy distribution (SED) of the ionizing continuum, especially the UV field. However, determining the SED is difficult since the line emitting gas might see a very different continuum from what we see (Korista et al. 1997). In the present calculation, we assumed a typical AGN continuum (i.e. the model AGN in CLOUDY), which is defined by a “big bump” with temperature $T = 1.5 \times 10^5$ K and a low-energy slope of $\alpha_{UV} = -0.5$, a typical value of X-ray to UV ratio $\alpha_{\text{OX}} = -1.4$ and an X-ray power-law with spectral index of $\alpha = -1$. As discussed in Section 3.2, the density of the material is high and it was taken in the range of $n_{\text{H}} = 10^8 - 10^{13} \text{ cm}^{-3}$ in our calculation. The low values of the G ratio indicate a low column density for the gas (Porter & Ferland 2007), and we adopted the value in the range of $N_{\text{H}} = 10^{19} - 10^{23} \text{ cm}^{-2}$. The ionization parameter is set in the range of $\log \xi \text{ (erg cm s}^{-1}\text{)} = 1 - 4$. Based on the width of the Ne X RRC, the temperature was fixed to $kT_e = 3 \text{ eV}$ in the calculation. In the analysis of the LETG spectrum of 3C 445, Reeves et al. (2010) found some tentative evidence for super-solar abundances of Mg and Si (2.6 and 6.5 times the solar value respectively), and this is confirmed by *Suzaku* observations (Braitto et al. 2011). Thus we assumed the same abundances as previous researches for Mg and Si, while the other abundances were fixed to the solar value.

A grid of emission line spectra was generated and incorporated into the partial covering model, and fitted to the overall spectra. The Si $K\alpha$ line was still modeled with a single Gaussian. This model provides a better fit to the HETG spectra than the collisional model, with the final overall fit statistic $C/\text{dof} = 1454/1290$. When adding a second photoionized component to the overall spectra, the statistic only improves by $\Delta C = 1$ for four parameters. This suggests a second component is not formally required. Thus the results are obtained with only one photoionized component. Figure 6 shows that the model gives a reasonable fit to the emission lines in the Mg and Si band.

5 RESULTS AND DISCUSSION

The overall fitted spectrum with the photoionization model is shown in Figure 7, and the best-fit parameters are listed in Table 2. Parameters for the continuum are basically consistent with previous measurements with

LETG or *Suzaku* data (Reeves et al. 2010; Braitto et al. 2011), except for the photon index of the primary power-law. The value $\Gamma = 1.4_{-0.3}^{+0.3}$ is lower than the typical value for BLRG objects ($\Gamma = 1.74_{-0.3}^{+0.3}$) (Grandi et al. 2004), indicating a hard/flat continuum. This is probably due to low quality of the data in the soft X-ray band. Given the uncertainty in the value, the photon index is roughly consistent with the typical value for BLRGs.

According to the ionization parameter, the photoionized component detected here corresponds to the second component detected in the LETG spectrum (i.e. the higher-ionization zone, see Reeves et al. 2010). A small column density of $N_{\text{H}} = 2.5_{-1.7}^{+3.8} \times 10^{20} \text{ cm}^{-2}$ was found for the line emitting gas, which is consistent with the values derived from several recent high-resolution soft X-ray spectra of Seyfert galaxies (e.g. Mrk 573, Gonzalez-Martin et al. 2010; Mrk 335, Longinotti et al. 2008 or NGC 1068, Kraemer et al. 2015). A high hydrogen density was found with $n_{\text{H}} = 5_{-4.5}^{+15} \times 10^{10} \text{ cm}^{-3}$, which is consistent with the analysis of R ratios associated with the Mg XI and Si XIII He-like triplets in Section 3.2.

With the best-fit parameters, we can estimate the distance of the gas to the central source. The distance R can be obtained by the definition of the ionization parameter, i.e. $\xi = L_{\text{ion}}/n_{\text{H}}R^2$ (Tarter et al. 1969), where L_{ion} is the ionization luminosity in 1–1000 Ryd, and n_{H} is the hydrogen density. Based on the SED used here, we calculated the ratio between the ionization luminosity and the bolometric luminosity, i.e. luminosity ratio the 1–1000 Ryd range and the whole energy range. Using the bolometric luminosity of 3C 445 ($L_{\text{bol}} = 1.3 \times 10^{45} \text{ erg s}^{-1}$, Grandi et al. 2006), the ionization luminosity was determined to be $L_{\text{ion}} = 3.6 \times 10^{44} \text{ erg s}^{-1}$. Then the radial distance was derived as $R \sim 1.9 \times 10^{15} \text{ cm}$ ($6 \times 10^{-4} \text{ pc}$). Considering the uncertainties in the parameters, the distance was ultimately determined to lie in the range $6 \times 10^{14} - 8 \times 10^{15} \text{ cm}$. Interestingly, the range is well within the optical BLR of 3C 445 with $R = 1.2 \times 10^{16} \text{ cm}$ (Osterbrock et al. 1976), suggesting we might be viewing the inner part of the BLR. Indeed, the best-fit hydrogen density is consistent with the typical value of the BLR in AGNs ($10^8 - 10^{12} \text{ cm}^{-3}$; Gonzalez-Martin et al. 2010, Longinotti et al. 2010). Moreover, as discussed in Section 3, the FWHM ratio of Si XIV and H β is consistent with 1 at the two-parameter 99% confidence level, which also supports the soft X-ray emitting gas being located in the BLR.

As shown in Figure 7, the strong Fe $K\alpha$ line can be modeled well by the reflection component (*reflion*),

Table 2 Summary of the Overall Spectral Modeling Parameters

Model Name	Parameter	Value
Power-law	Γ	$1.4^{+0.3}_{-0.3}$
	Normalization	$2.7^{+2.3}_{-1.3} \times 10^{-3}$
Scattered Power-law	Normalization	$7.2^{+1.0}_{-1.1} \times 10^{-5}$
Ionized reflection	ξ^a	10 erg cm s^{-1}
	Normalization	$1.2^{+0.3}_{-0.3} \times 10^{-5}$
Absorber1	N_H	$6.4^{+1.3}_{-1.3} \times 10^{22} \text{ cm}^{-2}$
Absorber2	N_H	$2.4^{+0.7}_{-0.6} \times 10^{23} \text{ cm}^{-2}$
	CvrFract ^b	$0.76^{+0.06}_{-0.09}$
Photoionization model	$\log \xi^c$	$3.3^{+0.4}_{-0.3}$
	N_H	$2.5^{+3.8}_{-1.7} \times 10^{20} \text{ cm}^{-2}$
	n_H	$5^{+15}_{-4.5} \times 10^{10} \text{ cm}^{-3}$

Notes: ^a The ionization parameter of the reflection component, fixed to the minimum value in the overall fitting; ^b Covering factor of the second absorbing component; ^c The ionization parameter in units of erg cm s^{-1} .

confirming the line originating from reflection off the Compton-thick matter detected in previous observations (Grandi et al. 2006; Braito et al. 2011). We estimated the location of this line emitting gas using its measured line width, i.e. $v_{\text{FWHM}} \sim 4100^{+2300}_{-1400} \text{ km s}^{-1}$ determined in the HEG spectrum. Assuming Keplerian motion, the distance of the gas to the central engine can be estimated as $R = GM/v^2$, where M is the mass of the central black hole in 3C 445 (which has an estimated value of $2 \times 10^8 M_{\odot}$; Grandi et al. 2006). The velocity dispersion v is related to FWHM velocity as $v^2 = \frac{3}{4}v_{\text{FWHM}}^2$. Thus we inferred the distance $R \sim 2 \times 10^{17} \text{ cm}$, comparable with the size of the optical BLR ($R = 1.2 \times 10^{16} \text{ cm}$; Osterbrock et al. 1976). This indicates that the Fe $K\alpha$ line probably originates from the BLR or outer region of the accretion disk. Using the same method, we estimated the distance of the Si $K\alpha$ line emitting gas to be $R > 2 \times 10^{18} \text{ cm}$ ($> 1 \text{ pc}$), which is consistent with the putative parsec-scale torus.

Our best-fit model seems to confirm the inner geometry of 3C 445 as proposed in Reeves et al. (2010). The central primary X-ray source is heavily absorbed by clumped and neutral/low-ionized matter (with column density of $\sim 10^{23} \text{ cm}^{-2}$), which may extend to the putative torus. Conversely, the soft X-ray or optical line emitting clouds are unobscured by the absorber, which is most probably due to these clouds being lifted above the plane of the accretion disk. Thus the clouds are photoionized by the central source and generate soft X-ray or optical emission lines. Meanwhile, they scatter the primary X-ray continuum into our line of sight (with the scattered power-law in Table 2). This structure is very similar to that observed in Seyfert 2 galaxies. One of the

most notable examples is the Seyfert 2 galaxy Mkn 3, in which broad optical emission lines are observed in polarized light (Miller & Goodrich 1990; Tran 1995), suggesting the BLR in this object is scattering the primary radiation into our line of sight. The main difference is that we are directly viewing the BLR of 3C 445, while the BLR is obscured in Mkn 3.

6 SUMMARY

Using the high resolution *Chandra* HETG spectrum, we have analyzed the soft X-ray emission for the BLRG object 3C 445. Highly ionized emission features are significantly detected and identified from H- or He-like Ne, Mg, Si and S ions. A prominent neutral Si $K\alpha$ line was also identified in the spectrum, which was supposed to originate from Compton-thick matter existing in 3C 445. We measured the centroid energy, fluxes, widths and equivalent widths of these features, and modeled the spectrum with both a collisional model and a photoionization model. The main results are as follows:

- (1) Most of the features are detected with a confidence level $> 99\%$. Most of the measured line centroid energy is consistent with experimental values, suggesting no velocity shift is required for the emitter. The measured line FWHMs are consistent with the $H\beta$ FWHM (3000 km s^{-1}) at the two-parameter 99% confidence level. The high values of the R ratios ($R = 0.9^{+1.1}_{-0.5}$ and $1.3^{+2.3}_{-0.7}$ for Mg XI and Si XIII respectively) suggest a high density for the line emitting matter.
- (2) A relatively weak Ne X RRC feature is detected in the spectrum. The narrow RRC feature indicates the

electron temperature of the line emitter is low (with $kT_e < 4$ eV). This supports a photoionization origin for the highly-ionized emission lines.

- (3) The G ratios of He-like lines indicate the emission lines originate from collisionally ionized plasmas. However, modeling the spectrum with a collisional ionization model fails to account for the emission lines present in the spectrum. This excludes a collisional origin for the emission lines.
- (4) A photoionization model succeeded in modeling the spectrum, with the best-fit parameters $\log \xi = 3.3^{+0.4}_{-0.3}$ erg cm s⁻¹, $n_H = 5^{+15}_{-4.5} \times 10^{10}$ cm⁻³ and $N_H = 2.5^{+3.8}_{-1.7} \times 10^{20}$ cm⁻². The high density of the emitter, the line FWHMs and the inferred radial distance all suggest the emitter is located in the BLR of 3C 445.

Acknowledgements We gratefully acknowledge the anonymous referee for helpful suggestions that improved the presentation of this manuscript. This work is based on observations made by the *Chandra* X-ray Observatory, and has made use of the CIAO software provided by the *Chandra* X-ray Center.

References

- Armentrout, B. K., Kraemer, S. B., & Turner, T. J. 2007, *ApJ*, 665, 237
- Bianchi, S., Guainazzi, M., & Chiaberge, M. 2006, *A&A*, 448, 499
- Braito, V., Reeves, J. N., Sambruna, R. M., & Gofford, J. 2011, *MNRAS*, 414, 2739
- Cash, W. 1979, *ApJ*, 228, 939
- Dere, K. P., Landi, E., Young, P. R., & Del Zanna, G. 2001, *ApJS*, 134, 331
- Dickey, J. M., & Lockman, F. J. 1990, *ARA&A*, 28, 215
- Eracleous, M., & Halpern, J. P. 2004, *ApJS*, 150, 181
- Ferland, G. J., Porter, R. L., van Hoof, P. A. M., et al. 2013, *RMxAA*, 49, 137
- Freeman, P., Doe, S., & Siemiginowska, A. 2001, in *Proc. SPIE*, 4477, *Astronomical Data Analysis*, ed. J.-L. Starck & F. D. Murtagh, 76
- Fruscione, A., McDowell, J. C., Allen, G. E., et al. 2006, in *Proc. SPIE*, 6270, *Society of Photo-Optical Instrumentation Engineers (SPIE) Conference Series*, 62701V
- Gabriel, A. H., & Jordan, C. 1969, *MNRAS*, 145, 241
- Gabriel, A. H., & Jordan, C. 1973, *ApJ*, 186, 327
- Gonzalez-Martin, O., Acosta-Pulido, J. A., Perez Garcia, A. M., & Ramos Almeida, C. 2010, *ApJ*, 723, 1748
- Grandi, P., Fiacchi, M., Palumbo, G. G. C., et al. 2004, in *IAU Symposium*, 222, *The Interplay Among Black Holes, Stars and ISM in Galactic Nuclei*, eds. T. Storchi-Bergmann, L. C. Ho, & H. R. Schmitt, 101
- Grandi, P., Malaguti, G., & Fiacchi, M. 2006, *ApJ*, 642, 113
- Grandi, P., Guainazzi, M., Cappi, M., & Ponti, G. 2007, *MNRAS*, 381, L21
- Gu, M. F. 2003, *ApJ*, 582, 1241
- Guainazzi, M., & Bianchi, S. 2007, *MNRAS*, 374, 1290
- Kaspi, S., Brandt, W. N., Netzer, H., et al. 2001, *ApJ*, 554, 216
- Kinkhabwala, A., Sako, M., Behar, E., et al. 2002, *ApJ*, 575, 732
- Korista, K., Ferland, G., & Baldwin, J. 1997, *ApJ*, 487, 555
- Kraemer, S. B., Schmitt, H. R., & Crenshaw, D. M. 2008, *ApJ*, 679, 1128
- Kraemer, S. B., Sharma, N., Turner, T. J., George, I. M., & Crenshaw, D. M. 2015, *ApJ*, 798, 53
- Kronberg, P. P., Wielebinski, R., & Graham, D. A. 1986, *A&A*, 169, 63
- Liedahl, D. A. 1999, in *Lecture Notes in Physics*, Berlin Springer Verlag, 520, *X-Ray Spectroscopy in Astrophysics*, eds. J. van Paradijs, & J. A. M. Bleeker, 189
- Liedahl, D. A., Osterheld, A. L., & Goldstein, W. H. 1995, *ApJ*, 438, L115
- Liedahl, D. A., & Paerels, F. 1996, *ApJ*, 468, L33
- Longinotti, A. L., Nucita, A., Santos-Lleo, M., & Guainazzi, M. 2008, *A&A*, 484, 311
- Longinotti, A. L., Costantini, E., Petrucci, P. O., et al. 2010, *A&A*, 510, A92
- Mewe, R., Lemen, J. R., & van den Oord, G. H. J. 1986, *A&AS*, 65, 511
- Miller, J. S., & Goodrich, R. W. 1990, *ApJ*, 355, 456
- Nucita, A. A., Guainazzi, M., Longinotti, A. L., et al. 2010, *A&A*, 515, A47
- Osterbrock, D. E., Koski, A. T., & Phillips, M. M. 1976, *ApJ*, 206, 898
- Piconcelli, E., Bianchi, S., Miniutti, G., et al. 2008, *A&A*, 480, 671
- Porquet, D., & Dubau, J. 2000, *A&AS*, 143, 495
- Porquet, D., Mewe, R., Dubau, J., Raassen, A. J. J., & Kaastra, J. S. 2001, *A&A*, 376, 1113
- Porter, R. L., & Ferland, G. J. 2007, *ApJ*, 664, 586
- Reeves, J. N., Gofford, J., Braito, V., & Sambruna, R. 2010, *ApJ*, 725, 803
- Sambruna, R. M., Reeves, J. N., & Braito, V. 2007, *ApJ*, 665, 1030
- Shu, X. W., Yaqoob, T., & Wang, J. X. 2010, *ApJS*, 187, 581
- Shu, X. W., Yaqoob, T., & Wang, J. X. 2011, *ApJ*, 738, 147
- Tarter, C. B., Tucker, W. H., & Salpeter, E. E. 1969, *ApJ*, 156, 943
- Torresi, E., Grandi, P., Guainazzi, M., et al. 2009, *A&A*, 498, 61
- Tran, H. D. 1995, *ApJ*, 440, 565
- Young, A. J., Wilson, A. S., & Shopbell, P. L. 2001, *ApJ*, 556, 6